HHS Public Access

Author manuscript

Inorg Chem. Author manuscript; available in PMC 2020 February 18.

Published in final edited form as:

Inorg Chem. 2019 February 18; 58(4): 2761–2769. doi:10.1021/acs.inorgchem.8b03344.

Redox and "Antioxidant" Properties of $Fe_2(\mu\text{-}SH)_2(CO)_4(PPh_3)_2$

Husain N. Kagalwala, **Noemie Lalaoui**, **Qian-Li Li**[‡], **Liang Liu**, **Toby Woods**, and **Thomas B. Rauchfuss**[*]

School of Chemical Sciences University of Illinois Urbana, IL 61801, USA

[‡]Department of Chemistry, Liaocheng University, Shandong, PRC 252059

Abstract

The chemistry of $Fe_2(\mu\text{-}SH)_2(CO)_4(PPh_3)_2$ (**2**$^{\mathbf{HH}}$) is described with attention to S-S coupling reactions. Produced by reduction of **2** ($Fe_2(\mu\text{-}S_2)(CO)_4(PPh_3)_2$), **2**$^{\mathbf{HH}}$ is an analogue of $Fe_2(\mu\text{-}SH)_2(CO)_6$ (**1**$^{\mathbf{HH}}$) that exhibits well-behaved S-centered redox. Both **2**$^{\mathbf{HH}}$ and the related **2**$^{\mathbf{MeH}}$ exist as isomers that differ with respect to the stereochemistry of the μ-SR ligands (R = H, Me). Compounds **2**$^{\mathbf{HH}}$, **2**$^{\mathbf{MeH}}$, and **2** protonate to give rare examples of Fe-SH-hydrides and Fe-S_2-hydrides. Salts of $[H\mathbf{2}]^+$, $[H\mathbf{2}^{\mathbf{HH}}]^+$, and $[H\mathbf{2}^{\mathbf{MeH}}]^+$ were characterized crystallographically. Complex **2**$^{\mathbf{HH}}$ reduces O_2, H_2O_2, $(PhCO_2)_2$, and Ph_2N_2 giving **2**. Related reactions involving **1**$^{\mathbf{HH}}$ gave uncharacterizable polymers. The differing behaviors of **2**$^{\mathbf{HH}}$ vs **1**$^{\mathbf{HH}}$ reflects the stabilization of the ferrous intermediates by the PPh_3 ligands. When independently generated by reaction of **2**$^{\mathbf{HH}}$ with TEMPO, **2*** quantitatively converts to **2** or, in the presence of C_2H_4, is trapped as the ethanedithiolate $Fe_2(\mu\text{-}S_2C_2H_4)(CO)_4(PPh_3)_2$. Evidence is presented that the Hieber-Gruber synthesis of **1** involves *poly*sulfido intermediates $[Fe_2(\mu\text{-}S_n)_2(CO)_6]^{2-}$ ($n > 1$). Two relevant experiments are: (i) protonation of $[Fe_4(\mu\text{-}S)_2(\mu\text{-}S_2)CO)_{12}]^{2-}$ gives **1** and **1**$^{\mathbf{HH}}$ and (ii) oxidation of **1**$^{\mathbf{HH}}$ by sulfur gives **1**.

Graphical Abstract

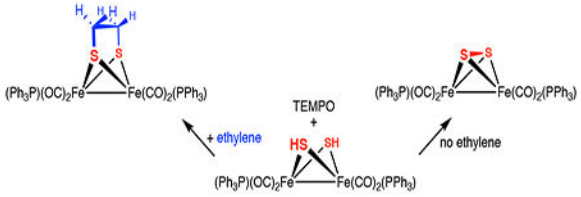

[*]**Corresponding Authors:** rauchfuz@illinois.edu.

Supporting Information

Spectroscopic data, selected reaction schemes, selected procedures.

SUPPORTING INFORMATION

The Supporting Information is available free of charge on the ACS Publications website at DOI: _

Accession Codes

CCDC 1877173, 1877177, 1877175, 1877176 contain the supplementary crystallographic data for this paper. These data can be obtained free of charge via www.ccdc.cam.ac.uk/data_request/cif, or by emailing data_request@ccdc.cam.ac.uk, or by contacting The Cambridge Crystallographic Data Centre, 12 Union Road, Cambridge CB2 1EZ, UK; fax: +44 1223 336033.

Introduction

The S-H bond of organic thiols is known to be relatively weak, with bond dissociation energies near 70 kcal/mol.[1] Indeed this weakness is widely exploited since thiols serve as antioxidants and inhibit radical reactions. The thiol-ene reaction is a route to useful polymers that exploits the addition of thiyl radicals to alkenes.[2] Given this rich background, the corresponding homolysis of the S-H bond of metallothiols (L_nMSH) is a likely reaction, especially since electropositive metal centers might be expected to stabilize S-centered radicals, leading to even weaker S-H than those quoted for organosulfur compounds.[3]

Of the many metallothiol complexes,[4,5] those of iron are of greatest interest because of their pervasiveness. The reactivity of FeS-H bonds is relevant to contemporary questions in bioinorganic chemistry. It is fairly certain that Fe-SH intermediates are involved in the biosynthesis of all Fe-S cofactors.[6] This assertion rests on the fact that the second pK_a of H_2S is near or above 14.[7] Consequently, all M-S forming reactions attributed to "sulfide" are in fact effected by SH^-. A specific functional role of an SH^- cofactor has recently been implicated in nitrogenase.[8,9] Finally, the FeSH/FeSSFe couple is invoked in the Iron-Sulfur Theory of evolution.[10]

To examine the radical properties of metallothiols, we selected $Fe_2(\mu\text{-}SH)_2(CO)_6$ (**1**$^{\mathbf{HH}}$).[11] Although only one of many Fe-SH complexes (Figure 1), $Fe_2(\mu\text{-}SH)_2(CO)_6$ is is the most studied metallothiol.[12–15]

While this project began with an intended focus on $Fe_2(\mu\text{-}SH)_2(CO)_6$, it quickly became apparent that this complex oxidizes (dehydrogenates) to uncharacterizable insoluble solids. Fortunately, the closely related derivative $Fe_2(\mu\text{-}SH)_2(CO)_4(PPh_3)_2$ exhibits the reversible S-centered reactivity that we sought. Of specific interest is the possibility that $Fe_2(\mu\text{-}SH)_2$ species might possess antioxidant behavior, akin to but extending that of glutathione and thioredoxin. In the present context, "antioxidant' is a chemical agent that reduces reactive oxygen species (ROS).[20,21] A well behaved antioxidant is one that generates a well-defined, ideally recyclable oxidized product upon exposure to the ROS. As demonstrated in this work, the $Fe_2(SH)_2$ group is a well-behaved antioxidant (Scheme 1).

Results

I. Characterization of $Fe_2(\mu\text{-}S_2)(CO)_4(PPh_3)_2$ and Related Compounds.

$Fe_2(\mu\text{-}S_2)(CO)_{6\text{-}x}(PPh_3)_x$ (x = 1, 2).—The disubstituted complex $Fe_2(\mu\text{-}S$ 2) $(CO)_4(PPh_3)_2$ (**2**) was prepared in 15–40% yield by substitution of the CO ligand in $Fe_2(\mu\text{-}S_2)(CO)_6$ (**1**) by PPh_3. The monophosphine complex $Fe_2(\mu\text{-}S_2)(CO)_5(PPh_3)$ (**3**) has been prepared previously.[22]

Compound **2** is well-behaved in solution. A single isomer was observed by ^{31}P NMR spectroscopy. Its structure was confirmed by X-ray crystallography (Figure 2). The structure of **2** has also been reported by Gao et al.[23] Compared to **1**,[24] the Fe-CO bonds in **2** are shorter by 0.05 Å, consistent with strengthened π-bonding. Curiously a valence isomer of **3**,

the diferrous sulfide $Fe_2(\mu\text{-}S)_2(CO)_4(PPh_3)_2$ has also been claimed on the basis of X-ray crystallography,[25] but we see no evidence for such a species.

$[HFe_2(\mu\text{-}S_2)(CO)_4(PPh_3)_2]^+$.—Protonation of the simplest diiron dithiolates of $Fe_2(\mu\text{-}SR)_2(CO)_4(PR_3)_2$ is well studied for many phosphine derivatives.[26,27] Usually protonation causes changes in stereochemistry. Two scenarios have been elucidated:

- Protonation of chelating dithiolates $Fe_2(\mu\text{-xdt})(CO)_4(PR'_3)_2$ causes the phosphine ligands to shift to basal sites (xdt = edt and pdt).[26,28]
- Protonation of bis(alkylthiolate)s $Fe_2(\mu\text{-}SR)_2(CO)_4(PR'_3)_2$ proceeds with no repositioning of the phosphines but a change in stereochemistry of the thiolate substituents R. In $Fe_2(\mu\text{-}SR)_2(CO)_4(PR'_3)_2$ (R = Me,[29] Et[28]), the S*R* groups are diequatorial.

The $Fe_2(S_2)(CO)_4(PPh_3)_2$ case follows neither pattern (eq 1).

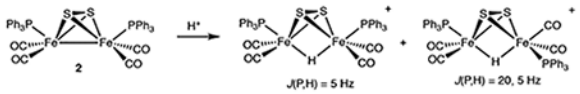

(1)

Treatment of CH_2Cl_2 solutions of **2** with $H(OEt_2)_2BAr^F{}_4$ resulted in a lightening of the solution color indicating protonation to give $[H\mathbf{2}]^+$. Excess acid had no effect. In the FT-IR spectrum, the ν_{CO} bands exhibited the expected shift of ca. 60–90 cm^{-1} toward higher energy. The magnitude of $\Delta\nu_{CO}$ indicate that protonation occurs at the Fe-Fe bond, not at sulfur. For comparison, $\Delta\nu_{CO}$ of 90 cm^{-1} is observed for the protonation of $Fe_2(\mu\text{-pdt})(CO)_4(PMe_3)_2$ to give $[(\mu\text{-H})Fe_2(\mu\text{-pdt})(CO)_4(PMe_3)_2]^+$.[27,28]

Two isomers of $[H\mathbf{2}]^+$ are indicated by both ^1H and ^{31}P NMR spectroscopy. Two sets of hydride signals appear in a 3:2 ratio, at −19.8 (dd, J = 20, 5 Hz) and −20.6 (t, J = 5 Hz). Accordingly, two sets of ^{31}P NMR signals are observed, and the HMBC experiment indicates the hydrides couple to distinct ^{31}P signals (Figure S6). The stereochemistry of the two isomers can be assigned by the splitting of the hydride signals: small values of $J(^{31}P,^1H)$ are typically observed for phosphines trans (apical sites) to μ-hydride, and larger values (~20 Hz) are observed for cis (basal sites).[30]

Persulfido hydrido complexes are rare, the precedents being $Cp^*{}_2Ta(S_2)H$ and its $Cr(CO)_5$ adduct.[31] The cation $[H\mathbf{2}]^+$ is the first example of an iron persulfido hydride. Its valence isomer $[Fe_2(\mu\text{-S})(\mu\text{-SH})(CO)_4(PPh_3)_2]^+$ would be an analogue of our recently reported $[Fe_2(\mu\text{-S})(\mu\text{-}SCH_2Ph)(CO)_2(dppv)_2]^+$.[32] X-ray crystallographic analysis confirmed the structure of $[H\mathbf{2}]^+$ (Figure 3). Compared to its conjugate base $Fe_2(\mu\text{-S 2})(CO)_4(PPh_3)_2$ (Supporting Information), the Fe-Fe distance in the hydride cation is elongated by almost 0.1 Å, from 2.5558(5) to 2.6326(5) Å. Compared to **2**, the Fe-CO bond distances are elongated by ~0.03 Å.

II. $Fe_2(\mu\text{-}SH)_2(CO)_4(PPh_3)_2$ and Related Compounds.

$Fe_2(\mu\text{-}SH)_2(CO)_4(PPh_3)_2$ and $Fe_2(\mu\text{-}SH)_2(CO)_5(PPh_3)$.—Compounds **2** and **3** undergo reductive conversion to the respective $(SH)_2$-containing derivatives, $Fe_2(\mu\text{-}SH)_2(CO)_{6\text{-}x}(PPh_3)_x$, $\mathbf{2^{HH}}$ and $\mathbf{3^{HH}}$. The conversion followed Seyferth's protocol ($LiBHEt_3$ reduction followed by trifluoroacetic acid).[11] Of course, **2** and **3** are unreactive toward H_2 (1 atm).

Both $\mathbf{2^{HH}}$ and $\mathbf{3^{HH}}$ exist of three isomers, which differ in terms of the stereochemistry of the SH groups (Table 1).[33] The rationale for the assignment of these isomers is presented in a subsequent section of this paper. The triplet at δ−0.79 is assigned to the ee isomer, the singlet at δ −0.16 and the triplet at δ −3.84 (J = 5 Hz) can be assigned respectively to the axial-equatorial isomer ae, and the triplet at d-4.55 (J = 5 Hz) is assigned to aa. Related to $\mathbf{3^{HH}}$, the complex $Fe_2(\mu\text{-}SH)_2(CO)_5(PhP(CH_2OH)_2)$ also consists of three isomers, with a ratio similar to that of $\mathbf{2^{HH}}$.[33]

$[HFe_2(\mu\text{-}SH)_2(CO)_4(PPh_3)_2]^+$.—Solutions of $\mathbf{2^{HH}}$ react with one equiv of $H(OEt_2)_2BAr^F{}_4$ at −80°C. The initial product is the hydride $[HFe_2(\mu\text{-}SH)_2(CO)_4(PPh_3)_2]^+$ ($[H\mathbf{2^{HH}}]^+$). The closest precedent to $[H\mathbf{2^{HH}}]^+$ is the radical $(\mu\text{-}H)Fe_2(\mu\text{-}SH)_2(CO)_6$, one of several products obtained by UV-irradiation of pentane solution of $Fe(CO)_5$ and H_2S at low-temperatures.[34] The structure of $[(\mu\text{-}H)Fe_2(\mu\text{-}SH)_2(CO)_4(PPh_3)_2]BAr^F{}_4$ was confirmed by X-ray crystallography (Figure 4). The ae and ee isomers cocrystallized.

Two isomers of $[H\mathbf{2^{HH}}]^+$ are indicted by the hydride signals at δ−17.0 and −17.6 as well as ^{31}P NMR singlets at δ 59.5 and 56.5 (−20°C). The isomer ratio is 1:1. The small value of J(H,P) indicates that the phosphines are diapical in each isomer. HMBC measurements indicate that the isomers differ with respect to the relative orientation of the SH groups (Figure S14), consisting of an unsymmetrical ae and a symmetrical isomer (Scheme 2). For the symmetrical isomer, only one S*H* signal correlated with one ^{31}P NMR signal whereas for the unsymmetrical isomer, two S*H* signals correlate with the second ^{31}P NMR signal. The symmetrical isomer is probably ee, the favored stereochemistry in other complexes of the type $[HFe_2(\mu\text{-}SR)_2(CO)_4(PR'_3)_2]^+$ (R = Me, Et).[28,29] The stabilization of the ee isomer is possibly associated with the shortened S ⋯S distances (by 0.1 Å) induced by ~0.05 Å protonation-induced elongation of the Fe⋯Fe distances.

Upon warming the solution to near 0°C, decomposition was evident by the evolution of gas. Gas chromatographic analysis showed that the gas was a mixture of H2 and CO. The main organometallic product of the decomposition is $\mathbf{2^{HH}}$, which forms in ~50% yield.

$Fe_2(\mu\text{-}SH)(\mu\text{-}SMe)(CO)_4(PPh_3)_2$ and $[HFe_2(\mu\text{-}SH)(\mu\text{-}SMe)(CO)_4(PPh_3)_2]^+$.—A mixed SH-SMe complex was prepared in the form of $Fe_2(\mu\text{-}SH)(\mu\text{-}SMe)(CO)_4(PPh_3)_2$ ($\mathbf{2^{MeH}}$). The complex was obtained by the addition of an excess of MeLi to **2** followed by acidification. The presumed intermediate in this reaction is $[Fe_2(\mu\text{-}SLi)(\mu\text{-}SMe)(CO)_4(PPh_3)_2]$.

The NMR properties of $\mathbf{2^{MeH}}$ are sufficiently definitive to allow not only the assignment of these isomers to structures, but also the assignments for $Fe_2(\mu\text{-}SH)_2(CO)_{6\text{-}}x(PPh_3)_x$, for

which consistent, logical assignments are lacking.[12] According to ^{1}H and ^{31}P NMR analysis, **2^{MeH}** consists of three isomers (Figure 5).

Four isomers are possible: $a^{H}e^{Me}$, $e^{H}e^{Me}$, and $e^{H}a^{Me}$, $a^{H}a^{Me}$. The missing isomer must be $a^{H}a^{Me}$. The aa isomer is minor in **1^{HH}** and **2^{HH}**, and completely absent in $Fe_2(\mu\text{-}SMe)_2(CO)_6$,[35–38] which exists only as $e^{Me}e^{Me}$ and $a^{Me}e^{Me}$ (Scheme 3).[39,40] Apparently only the miniscule H substituent is compatible with the diaxial configuration.[41] We conclude that for **2^{MeH}** the aa isomer is destabilized by a steric clash. The relative chemical shifts of the SH signals and the magnitude of the ^{31}P-^{1}H couplings are consistent with the previous assignments.

Protonation of **2^{MeH}** gave an isolable hydride salt [H**2^{MeH}**]BF_4, which was characterized by X-ray crystallography (Figure 6). Crystallographic analysis of [H**2^{MeH}**]BF_4 revealed a single isomer with equatorial S*Me* and axial S*H*. As seen for $[HFe_2(\mu\text{-}SR)_2(CO)_4(PR'_3)_2]^+$ (R = Me,[29] Et[28]), the two phosphine ligands remain apical, reflecting the steric protection afforded by the single equatorial methyl group.

Compared to [H**2^{HH}**]$^+$, [H**2^{MeH}**]$^+$ is noticeably more stable in solution at room temperature. This enhanced stability is attributed in part to the greater electron releasing properties of the SMe^- vs SH^- groups. This trend is indicated by the relative values of ν_{CO} for **2^{HH}** vs **2^{MeH}**, which are 2000, 1955, 1938 and 1995, 1948, 1930 cm^{-1}, respectively.

III. Oxidation of $Fe_2(\mu\text{-}SH)_2(CO)_4(PPh_3)_2$.

Although **1^{HH}** has been described as “air-sensitive,” little is known about the products of air oxidation. When left open to air in THF solution, **1^{HH}** degrades over the course of hours to a black solid and ca. 50% yield of **1**. Under these conditions **1** is very stable in THF solution, so the black solid does not result from degradation of **1**. In solution, **2^{HH}** is more air-stable than **1**, but converts to **2** over the course of days. The conversion of **2^{HH}** into **2** proceeds quantitatively according to ^{31}P NMR spectroscopy.

Given the efficiency of the **2^{HH}** + O_2 reaction, other oxidants were examined. Azobenzene was found to react over the course of several hours at room temperature to generate diphenylhydrazine and **2**. The hydrogenation of azobenzene by iron sulfido complexes has not been reported, but the reaction is catalyzed by $(CH_3C_5H_4)_2Mo_2S_2(S_2CH_2)$.[42]

The O_2 + **2^{HH}** reaction is proposed to involve H-atom abstraction by O_2, leading sequentially to hydroperoxide (HO_2), H_2O_2, and H_2O. Using aqueous H_2O_2 in place of air, the conversion **2^{HH}** → **2** proceeds in minutes (vs days, eq 2).

$$\underset{\mathbf{2^{HH}}}{Fe_2(\mu\text{-}SH)_2(CO)_4(PPh_3)_2} + H_2O_2 \rightarrow \underset{\mathbf{2}}{Fe_2(\mu\text{-}S_2)(CO)_4(PPh_3)_2} + 2H_2O \quad (2)$$

Benzoyl peroxide ($(PhCO_2)_2$) is a very fast oxidant, the conversion being complete in the time of mixing.

IV. Mechanistic Studies on the Oxidation of $Fe_2(\mu\text{-}SH)_2(CO)_4(PPh_3)_2$.

To learn more about the O_2 + $\mathbf{2^{HH}}$ reaction, the reagent 2,2,6,6-tetramethyl-1-piperidinyloxy (TEMPO) was employed. Since it abstracts H atoms from weak X-H bonds,[43] TEMPO serves as a weighable surrogate of O_2 with enhanced reactivity. Within seconds of being treated with TEMPO, $\mathbf{2^{HH}}$ quantitatively converted into **2**. A deficiency of TEMPO resulted in partial conversion to **2**, leaving unreacted $\mathbf{2^{HH}}$. This result indicates that mixed valence species $Fe_2(\mu\text{-}SH)(\mu\text{-}S)CO)_4(PPh_3)_2$ ($\mathbf{2^{H}}$) is a superior H-atom donor relative to $\mathbf{2^{HH}}$ (Scheme 4).

These results are consistent with DFT-calculated bond dissociation free energies for $Fe_2(\mu\text{-}SH)_{2\text{-}x}(\mu\text{-}S)_x(CO)_6$. Those S-H bond energies are calculated to be 72 and 45 kcal/mol, respectively for $x = 0$ and $x = 1$.[44] Oxidation of $\mathbf{3^{HH}}$ with two equiv of TEMPO cleanly gave **3**. On the other hand, oxidation of $\mathbf{1^{HH}}$ with 0.5–2 equiv of TEMPO resulted in nearly full conversion to a black solid.

Trapping experiments implicate unsaturated intermediates in the TEMPO-induced dehydrogenation of $Fe_2(\mu\text{-}SH)_2(CO)_{6\text{-}x}(PPh_3)_x$. Addition of 2 equiv of TEMPO to an C_2H_4-saturated solution of $\mathbf{2^{HH}}$ gave a 1:3 mixture of **2** and the ethanedithiolate $Fe_2(\mu\text{-}S_2C_2H_4)(CO)_4(PPh_3)_2$, respectively. The identity of $Fe_2(\mu\text{-}S_2C_2H_4)(CO)_4(PPh_3)_2$ was verified by independent synthesis.[45] In a control experiment, C_2H_4 was shown to be unreactive toward **2**, i.e. no thermal reaction occurs (Scheme 5).

The TEMPO-C_2H_4-trapping experiments were extended to $\mathbf{3^{HH}}$ and $\mathbf{1^{HH}}$. Addition of two equiv of TEMPO to a C_2H_4-saturated solution of the monophosphine $\mathbf{3^{HH}}$ mainly produced black solids together with small amounts of the ethanedithiolate $Fe_2(\mu\text{-}S_2C_2H_4)(CO)_5(PPh_3)$ and **3** in a ratio of 1:9, based on ^{31}P NMR analysis. This ethanedithiolate was identified by independent synthesis ($Fe_2(\mu\text{-}S_2C_2H_4)(CO)_6$ + PPh_3). Its ^{1}H NMR spectrum is distinctive in the CH_2 region showing two multiplets, consistent with an AA'BB' coupling pattern where AA' and BB' correspond to H's facing toward or away from the PPh_3 ligand.

Trapping agents other than ethylene were tested without success. Treatment of solutions of $\mathbf{2^{HH}}$ with two equiv TEMPO under an atmosphere of D_2, in the presence of 10 equiv of $PhMe_2SiH$, phenylacetylene, or 1-hexene gave only **2**. Substituted alkenes are known to be unreactive toward UV-irradiated solutions of **1**.[46,47]

V. Synthetic Pathway Leading to $Fe_2(\mu\text{-}S_2)(CO)_6$.

The results described above are relevant to an old mystery: the pathway for the synthesis of **1**. Since it was reported in 1958 by Hieber and Gruber (H-G), the synthesis of **1** has remained unaddressed.[48] This oversight contrasts with the hundreds of studies that use **1**. The H-G synthesis involves the formation of an Fe-S-CO anion by the reaction of $[HFe(CO)_4]^-$ and sodium polysulfide (or elemental sulfur) followed by acidification. A key fact is that $\mathbf{1^{2-}}$ is not a precursor to **1**, it simply protonates to give $\mathbf{1^{HH}}$. The requirement of the H-G synthesis for excess sulfur provides the main clue to the pathway (Table 2). Although the H-G synthesis reaction does not involve $\mathbf{1^{2-}}$, this dianion can be used to

generate intermediates in the pathway of the H-G synthesis. Indeed, treating a THF solution of Li_2[**1**] with excess S (as S_8) followed by acid efficiently gave **1**.

The role of polysulfide intermediate(s) in the conversion of $\mathbf{1}^{2-}$ to **1** is supported by ^{13}C NMR studies. ^{13}C NMR spectroscopy allows the identification of $\mathbf{1}^{HH}$ and **1**, which are otherwise difficult to distinguish by FT-IR spectroscopy (Figure S26). The ^{13}C NMR spectrum of $\mathbf{1}^{HH}$ consists of three singlets (δ209.4, 209.2, 209.0), consistent with the presence of aa, ee, and ae isomers, respectively. The center signal, corresponding to a minor isomer, overlaps with the singlet for **1**. According to ^{13}C NMR spectroscopy, a THF solution of $\mathbf{1}^{HH}$ converts to **1** in the presence of elemental sulfur. Unlike the $\mathbf{1}^{HH}$ + O_2 reaction, the $\mathbf{1}^{HH}$ + S reaction is more efficient (no black solids). The $\mathbf{1}^{HH}$ + S → **1** conversion does not proceed in the presence of acid, so it is probably not relevant to the H-G synthesis.

Further insights were obtained using salts of the persulfide $[Fe_4S_4(CO)_{12}]^{2-}$.[49] In terms of their IR spectra, the species generated by the reaction of Li_2[**1**] with S is almost identical to $(BnNMe_3)_2[Fe_4S_4(CO)_{12}]$ (Figure 7). This salt was obtained by the addition of $BnNMe_3^+$ to a H-G synthesis solution. Treatment of MeCN solution of $(BnNMe_3)_2[Fe_4S_4(CO)_{12}]$ with excess *p*-toluene sulfonic acid (HOTs) gave an

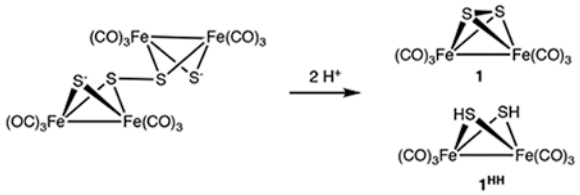

(3)

approximate 1:1 mixture of $\mathbf{1}^{HH}$ and **1** (Figure 8, eq 3). This finding is consistent with the hypothesis that *poly*sulfides derived from $[\mathbf{1}]^{2-}$ undergo ring-closure upon protonation to give **1**.

Summary and Conclusions

The work mainly examines the diiron dithiol $Fe_2(\mu\text{-}SH)_2(CO)_4(PPh_3)_2$ ($\mathbf{2}^{HH}$) as a well-behaved, readily interrogated analogue of $Fe_2(\mu\text{-}SH)_2(CO)_6$. Complex $\mathbf{2}^{HH}$ exhibits unusual redox properties resulting in hydrogen atom transfer, which regenerates the disulfide **2**. In this regard, the diiron dithiol exhibits well-behaved antioxidant behavior.

Why is $\mathbf{2}^{HH}$ a superior and better-behaved reductant relative to $\mathbf{1}^{HH}$? We propose that the PPh_3 ligands stabilize the dehydrogenated intermediate $Fe_2(\mu\text{-}S)_2(CO)_4(PPh_3)_2$ (**2***), which resists the addition of further equiv of $Fe_2(\mu\text{-}SH)_2(CO)_4(PPh_3)_2$. In contrast, $Fe_2(\mu\text{-}S)_2(CO)_6$ (**1***) consumes 1^{HH}, giving polymers competitive with conversion to **1**.

Both electronic and steric arguments can be used to rationalize the stability of **2***. Featuring ferrous centers, **2*** would be stabilized strongly by presence of phosphine ligands. Indicative of the effect of phosphine substitution, the reduction potentials for $[Fe_2(\mu\text{-}SR)_2(CO)_6]^+$ and

$[Fe_2(\mu\text{-}SR)_2(CO)_4(PPh_3)_2]^+$ differ by ~0.8 V.[50] Computational experiments indicate that the diferrous species $Fe_2(\mu\text{-}S)_2(CO)_6$, analogous to **2***, exists as a singlet ground state.[51] It is also possible that the stabilizing influence of the PPh_3 ligands is steric in origin, preventing **2*** from attacking $\mathbf{2^{HH}}$.

The trapping results using $\mathbf{2^{HH}}$/TEMPO/C_2H_4 reaction are reminiscent of the photochemical reactivity of **1**. UV-irradiation of **1** in presence of alkynes, ethylene, and CO gives $Fe_2(\mu\text{-}S_2C_2R_2)(CO)_6$,[52] $Fe_2(\mu\text{-}S_2C_2H_4)(CO)_6$, and $Fe_2(\mu\text{-}S_2CO)(CO)_6$, respectively.[22,46,47,53,54] The intermediate generated in the $\mathbf{1^{HH}}$/TEMPO and $\mathbf{1^{HH}}$/O_2 reactions appears to react with $\mathbf{1^{HH}}$ to give intractable solids. In contrast the intermediate **2*** generated in the corresponding oxidations of $Fe_2(\mu\text{-}SH)_2(CO)_4(PPh_3)_2$ does not add $\mathbf{2^{HH}}$ but cleanly converts to **2**.

Finally, the experiments on $\mathbf{1^{HH}}$ were extended to partially illuminate the final stages in the Hieber-Gruber synthesis of **1**. Acid-labile per- or polysulfides of the type $[Fe_2(\mu\text{-}S_n)_2(CO)_6]^{2-}$ or $[Fe_2(\mu\text{-}S)(\mu\text{-}S_n)(CO)_6]^{2-}$ are implicated ($n > 1$, Scheme 6). The salient findings are (i) $\mathbf{1^{HH}}$ + S_8 gives **1**, while $\mathbf{1^{HH}}$ + O_2 does not and (ii) $Fe_4(\mu\text{-}S)_2(\mu\text{-}S\ 2)(CO)_{12}]^{2-}$ + H^+ gives **1**, while $\mathbf{1^{2-}}$ + H^+ + does not.

Experimental

Materials and methods have been described recently.[32]

$Fe_2(S_2)(CO)_4(PPh_3)_2$ (2).

A 100-mL Schlenk flask was charged with 0.80 g (2.33 mmol) of **1** and 50 mL of THF to give a red-orange solution. At −78°C, addition of 1.22 g (4.66 mmol) of PPh_3 and 0.35 g (4.66 mmol) of Me_3NO. The solution was allowed to warm to room temperature over the course of several min. After 28 h, solvent was evaporated. The dark red residue was purified by chromatography on silica gel eluting with 1:10 CH_2Cl_2-hexanes. Three red bands eluted, the first being **1**, the second being **3**, and the third band was **2** (further unidentified products could be collected by eluting with CH_2Cl_2). Yield: 0.65 g (15–35%). IR (CH_2Cl_2): υ_{CO} 2000, 1950, 1935 cm^{-1}. ^1H NMR (500 MHz, CD_2Cl_2): δ 7.44–7.40, (m, 30H, PPh_3). ^{31}P NMR (CD_2Cl_2): δ 57.69 (s). Single X-ray crystals were grown from a concentrated pentane solution at −20°C. Anal. Calcd for $C_{40}H_{30}P_2Fe_2O_4S_2$: C, 59.13; H, 3.72. Found: C, 58.73; H, 3.69.

$[HFe_2(\mu\text{-}S_2)(CO)_4(PPh_3)_2]BAr^F{}_4$ ($[H2]BAr^F{}_4$).

A solution of 50 mg (0.06 mmol) of **2** in 2 mL of CH_2Cl_2 was treated with $H(OEt_2)_2BAr^F{}_4$ (62.3 mg, 0.06 mmol). Pentane was added, and the mixture was maintained at −20°C overnight. The resulting solid precipitate was washed with 10 mL of pentane. Yield: 87 mg (86%). IR (CH_2Cl_2): υ_{CO} 2061, 2041, 2008 cm^{-1}. ^1H NMR (500 MHz, CD_2Cl_2): δ 7.73–7.28 (m, 42 H), −19.80 (dd, J = 20 and 5 Hz, 0.37H, μ-H isomer A), −20.56 (t, J = 5Hz, 0.26 H, μ-H isomer B). ^{31}P NMR (CD_2Cl_2): δ 61.52, 61.55, 61.63, 61.66 (isomer B) and 55.5 (isomer A). Single X-ray crystals were grown from a concentrated CH_2Cl_2 solution layered with pentane at −20°C.

$Fe_2(\mu\text{-}SH)_2(CO)_4(PPh_3)_2$ (2^{HH}).

A stirred solution of 0.2 g (0.25 mmol) of **2** in 30 mL of THF at −78°C was treated dropwise with 0.62 mL (0.62 mmol) of $LiHBEt_3$. The initially red solution became green, indicating the formation of $(\mu\text{-}LiS)_2Fe_2(CO)_4(PPh_3)_2$. After the reaction mixture had stirred for an additional 15 min., 68 μL (0.90 mmol) of CF_3CO_2H was added, causing an immediate color change from green to red, indicating the formation of $\mathbf{2^{HH}}$. After stirring for an additional 15 min at −78°C, the mixture was concentrated in vacuo. The red gummy residue was extracted with ca. 15 mL of CH_2Cl_2, and this extract was passed through a plug of Celite. The solvent was evaporated under vacuum to afford a red solid. Yield: 0.18 g (90%). IR (CH_2Cl_2): υ_{CO} = 2000, 1955, 1938 cm^{-1}. ^1H NMR (500 MHz, CD_2Cl_2): δ 7.47–7.39 (m, 30H, PPh_3), −0.16 (s, e-H of ae isomer), −0.79 (s, e-H of ee isomer), −3.84 (s, a-H of ae isomer), −4.55 (s, a-H of aa isomer). ^{31}P NMR (CD_2Cl_2): δ 59.2 (s, aa), 55.2 (s, ae), 52.2 (s, ee). Single X-ray crystals were grown from a concentrated CH_2Cl_2 solution layered with pentane at −20°C. Anal. Calcd for C $40H_{32}Fe_2O_4P_2S_2$ CH_2Cl_2: C, 54.74; H, 3.81 Found: C, 55.14; H, 3.59.

$[HFe_2(\mu\text{-}SH)_2(CO)_4(PPh_3)_2]BAr^F{}_4$ ($[H2^{HH}]BAr^F{}_4$).

To a stirred solution of 30 mg (0.04 mmol) of $\mathbf{2^{HH}}$ in 1 mL of CD_2Cl_2 at - 80°C was added $H(OEt_2)_2BAr^F{}_4$ (37 mg, 0.04 mmol). IR (CH_2Cl_2): υ_{CO} 2061, 2041, 2008 cm^{-1}. ^1H NMR (500 MHz, CD_2Cl_2): δ δ 7.72–7.43 (m), −0.01 (s, e-H of ae isomer), −3.51 (s, a-H of ae isomer), −3.81 (s, a-H of aa isomer), −17.02 (br s, μ-H of aa isomer) and −17.63 (br s, μ-H of ae isomer). ^{31}P NMR (CD_2Cl_2): δ 59.5 (s, aa), 56.5 (s, ae).

$Fe_2(\mu\text{-}SMe)(\mu\text{-}SH)(CO)_4(PPh_3)_2$ (2^{MeH}).

A stirred solution of 0.0812 g (0.1 mmol) of **2** in 5 mL of THF at −78°C was treated with 0.19 mL (0.3 mmol, 1.6 M) of MeLi. The mixture assumed a dark green color attributed to $Fe_2(\mu\text{-}LiS)(\mu\text{-}SMe)(CO)_4(PPh_3)_2$. After being maintained at −78°C for 15 min, the reaction mixture was treated with 23 μL (0.3 mmol) of CF_3CO_2H, causing an immediate color change from green to red, consistent with the formation of $\mathbf{2^{MeH}}$. After an additional 15 min at −78°C, the mixture was allowed to warm to room temperature, and solvent was removed. The red gummy residue was extracted into ca. 2 mL of CH_2Cl_2, and this extract was filtered through a plug of Celite. The solvent was evaporated under vacuum to afford a dark red solid. Recrystallization of this solid was achieved by addition of pentane to a CH_2Cl_2 solution, followed by cooling to −20°C. Yield: 0.074 g (90%). Anal. Calcd for $C_{41}H_{34}Fe_2O_4P_2S_2$•0.5 CH_2Cl_2: C, 57.23; H, 4.05. Found: C, 57.01; H, 3.98. IR (CH_2Cl_2): υ_{CO} 1995, 1948, 1930 cm^{-1}. ^1H NMR (500 MHz, CD_2Cl_2): δ 7.53–7.38 (m, 45H, PPh_3), 1.35 (s, ae, e-CH_3), 1.25 (s, ee, e-CH_3), 0.07 (s, ea, a-CH_3), −0.73 (s, ee, e-H), −0.79 (s, ea, e-H), −3.73 (t, ae, a-H, J = 5Hz). ^{31}P NMR (CD_2Cl_2): δ 57.3 (s, ea, e-CH_3, a-H), 55.4 (s, ae, a-H, e-CH_3), 53.1 (s, ee, e-H, e-CH_3). Single X-ray crystals were grown by layering a concentrated CH_2Cl_2 solution with pentane at −20°C.

$[HFe_2(\mu\text{-}SMe)(\mu\text{-}SH)(CO)_4(PPh_3)_2]BAr^F{}_4$ ($[H2^{MeH}]BAr^F{}_4$).

A stirred solution of 0.0828 g (0.1 mmol) of $\mathbf{2^{MeH}}$ in 2 mL of CH_2Cl_2 was treated with 0.1012 g of $HBAr^F{}_4{\cdot}2Et_2O$, causing an immediate color change from dark read to light red. The product was purified by layering a concentrated CH_2Cl_2 solution (~0.5 mL) with 20 mL

of pentane at −20°C. Anal. Calcd for $C_{73}H_{47}Fe_2O_4P_2S_2BF_{24}$•0.5 CH~ $2Cl_2$: C, 50.88; H, 2.79. Found: C, 50.92; H, 2.52. IR (CH_2Cl_2): υ_{CO} 2099, 2055, 2040, 2003 cm^{-1}. ^1H NMR (500 MHz, CD_2Cl_2): δ 7.51–7.75 (m, 2 PPh_3 and $BAr^F{}_4$), 1.42, 1.38, 1.09, 0.99, 0.65, 0.14 (CH_3), −0.59, −0.70, −1.30, −1.53, −1.85, −2.97 (S-H), −15.51, −16.26, −16.35, −17.35 (m, μ-H). ^{31}P NMR (CD_2Cl_2): δ 56.6 (m), 51.9 (m), 51.2 (m), 50.2 (t), 50.5 (m), 43.1 (m). Single X-ray crystals were grown from a concentrated CH_2Cl_2 solution layered with pentane at −20°C.

Ethylene Trapping Reactions.

A solution of **2^{HH}** (50 mg, 0.06 mmol) in THF (15 mL) was cooled to 0°C and saturated with ethylene. A THF solution of TEMPO (0.61 M, 0.2 mL) was injected, and the mixture was stirred for an additional 30 min., maintaining the ethylene purge. Solvent was removed under vacuum, and the flask was taken into a glove box. The residue was dissolved in a minimum amount of DCM, and the solution was filtered to remove a small amount of insoluble material. Addition of pentane to the filtrate yielded a red-pink powder consisting of $Fe_2(S_2C_2H_4)(CO)_4(PPh_3)_2$ and **2**.[45] ^1H-NMR (CD_2Cl_2):δ 7.57 (m, 14H), 7.40 (m, 34H), 0.65 (s, 4H). ^{31}P NMR (CD_2Cl_2): δ 60.25 (s), 57.69 (s). When a solution of **2^{HH}** (50 mg, 0.06 mmol) in THF (15 mL) was treated with TEMPO (19 mg, 0.12 mmol), **2** was the exclusive product as demonstrated by ^{31}P NMR analysis and thin-layer chromatography.

$(BnNMe_3)_2[Fe_2S_2(CO)_6]_2$.

The modified procedure was based on the literature.[45] A solution of **1** (5.0 mmol, 1.72 g) in THF (10 mL) was treated dropwise with $LiBHEt_3$ (5.0 mmol, 5 mL, 1 M in THF) at −78°C. The solution turned to greenish dark immediately. After 30 min, a solution of $PhCH_2NMe_3Cl$ (5.0 mmol, 925 mg) in a mixture of MeCN (8 mL) and MeOH (2 mL) was added to the above solution. After stirring the mixture at −20°C for 1 h, solvents were removed under vacuum. The residue was washed with cold THF and Et_2O and dried under vacuum. Yield: 2.67 g (54%). IR (MeCN): υ_{CO} 2041, 2029, 2002, 1954 cm^{-1}. ^{13}C NMR (125 MHz, CD_3CN): δ 53.4, 70.2, 128.6, 130.1, 131.7, 133.8, 214.5.

Effect of S/Fe Ratio on Hieber-Gruber Synthesis.

A 500-mL flask was charged with $Fe(CO)_5$ (1.0 equiv, 14.8 mmol, 2 mL) and MeOH (12 mL) followed by aqueous KOH (50% w/w, 7.2 equiv, 6.0 g). After 10 min., the orange solution was cooled to 0°C. Elemental sulfur (x equiv, see Table 2) was added, producing a dark brown dark solution. *Caution:* gas evolution! After stirring for 1 h at 0°C, the mixture was treated with water (75 mL), pentane (100 mL), followed by solid NH_4Cl (10 equiv, 148 mmol, 8.0 g) in one portion. After being kept at 0°C for ca. 3 h, the solution was allowed to warm to room temperature overnight. The mixture was extracted exhaustively with pentane (in cases where phase separation was unclear, ~10 mL of acetone was added). The combined pentane extracts were filtered through a pad of silica gel and evaporated using a rotary evaporator. For purification by chromatography on silica gel, pentane alone was used. The first orange band was **1**, which was further purified by repeated evaporation-extraction into pentane to remove sulfur.

X-ray Crystallographic Determinations.

Crystallographic Data were collected on a Bruker D8 Venture instrument equipped with a four-circle kappa diffractometer and Photon 100 detector. An Iμs microfocus Mo (λ = 0.71073 Å) source was supplied the multi-mirror monochromated incident beam. The samples were mounted on a 0.3 mm loop with the minimal amount of Paratone-N oil. Data were collected as a series of φ and/or ω scans. Data were collected at 100K and integrated and filtered for statistical outliers using SAINT,[55] and corrected for absorption by multi-scan methods using SADABS[56] v2014/7. The structures were phased using direct methods[57] or intrinsic phasing methods[58] and then refined with the SHELX software package SHELX-2014–7.[57]

Supplementary Material

Refer to Web version on PubMed Central for supplementary material.

ACKNOWLEDGMENTS

This work was supported by GM-61153 from the National Institutes of Health.

REFERENCES

1. Luo YR Comprehensive Handbook of Chemical Bond Energies; CRC Press: Boca Raton, FL, 2007.
2. Dénès F; Pichowicz M; Povie G; Renaud P, Thiyl Radicals in Organic Synthesis. Chem. Rev 2014, 114, 2587–2693. [PubMed: 24383397]
3. Appel AM; Lee S-J; Franz JA; DuBois DL; Rakowski DuBois M, Free Energy Landscapes for S−H Bonds in $Cp^*_2Mo_2S_4$ Complexes. J. Am. Chem. Soc 2009, 131, 5224–5232. [PubMed: 19309157]
4. Kuwata S; Hidai M, Hydrosulfido Complexes of Transition Metals. Coord. Chem. Rev 2001, 213, 211–305.
5. Peruzzini M; de los Rios I; Romerosa A, Coordination Chemistry of Transition Metals with Hydrogen Chalcogenide and Hydrogen Chalcogenido Ligands. Prog. Inorg. Chem 2001, 49, 169–543.
6. Lill R, Function and Biogenesis of Iron-Sulfur Proteins. Nature 2009, 460, 831–838. [PubMed: 19675643]
7. Meyer B; Ward K; Koshlap K; Peter L, Second Dissociation Constant of Hydrogen Sulfide. Inorg. Chem 1983, 22, 2345–2346.
8. Hoffman BM; Lukoyanov D; Dean DR; Seefeldt LC, Nitrogenase: A Draft Mechanism. Acc. Chem. Res 2013, 46, 587–595. [PubMed: 23289741]
9. Khadka N; Milton RD; Shaw S; Lukoyanov D; Dean DR; Minteer SD; Raugei S; Hoffman BM; Seefeldt LC, Mechanism of Nitrogenase H_2 Formation by Metal-Hydride Protonation Probed by Mediated Electrocatalysis and H/D Isotope Effects. J. Am. Chem. Soc 2017, 139, 13518–13524. [PubMed: 28851217]
10. Wächtershäuser G, From Chemical Invariance to Genetic Variability In Bioinspired Catalysis; Weigand Wand Schollhammer P, 2014, Wiley-VCH, Weinheim.
11. Seyferth D; Henderson RS, Di-μ-Thiolbis(tricarbonyliron), $(\mu\text{-HS})_2Fe_2(CO)_6$: An Inorganic Mimic of Organic Thiols. J. Organomet. Chem 1981, 218, C34–C36.
12. Crouthers DJ; Ding S; Denny JA; Bethel RD; Hsieh C-H; Hall MB; Darensbourg MY, A Reduced 2Fe2S Cluster Probe of Sulfur-Hydrogen versus Sulfur-Gold Interactions. Angew. Chem., Int. Ed 2015, 54, 11102–11106.
13. Seyferth D; Womack GB; Henderson RS; Cowie M; Hames BW, Michael-Type Addition Reactions of Bis(*μ*-mercapto)bis(tricarbonyliron): Proximity-Induced Formation of Bidentate Organosulfur Ligands. Organometallics 1986, 5, 1568–1575.

14. Rauchfuss TB, Diiron Azadithiolates as Models for the [FeFe]-Hydrogenase Active Site and Paradigm for the Role of the Second Coordination Sphere. Acc. Chem. Res 2015, 48, 2107–2116. [PubMed: 26079848]
15. Li Y; Rauchfuss TB, Synthesis of Diiron(I) Dithiolato Carbonyl Complexes. Chem. Rev 2016, 116, 7043–7077. [PubMed: 27258046]
16. Arif AM; Hefner JG; Jones RA; Koschmieder SU, Mononuclear Complexes of Cr(II) and Fe(II) with Terminal -SH Groups. Synthesis and X-ray Crystal Structures of trans-$M(SH)_2(dmpe)_2$ (M = Cr, Fe; dmpe = 1,2-Bis(dimethylphosphino)ethane). J. Coord. Chem 1991, 23, 13–19.
17. Segal BM; Hoveyda HR; Holm RH, Terminal Ligand Assignments Based on Trends in Metal −Ligand Bond Lengths of Cubane-Type $[Fe_4S_4]^{2+,+}$Clusters. Inorg. Chem 1998, 37, 3440–3443.
18. Di Vaira M; Midollini S; Sacconi L, Synthesis, Properties, and X-Ray Characterization of 3d Metal-Mercapto and -Methylthio Complexes with the Poly(tertiary phosphines) Tris(2-diphenylphosphinoethyl)amine and Tris(2-diphenylphosphinoethyl)phosphine. Inorg. Chem 1977, 16, 1518–1524.
19. Tsou C-C; Chiu W-C; Ke C-H; Tsai J-C; Wang Y-M; Chiang M-H; Liaw W-F, Iron(III) Bound by Hydrosulfide Anion Ligands: NO-Promoted Stabilization of the $[Fe^{III}–SH]$ Motif. J. Am. Chem. Soc 2014, 136, 9424–9433. [PubMed: 24917476]
20. Deponte M, Glutathione catalysis and the reaction mechanisms of glutathione-dependent enzymes. Biochimi. Biophys. Acta 2013, 1830, 3217–3266.
21. Powis G; Montfort WR, Properties and Biological Activities of Thioredoxins. Ann. Rev. Biophys. Biomolec. Struct 2001, 30, 421–455.
22. Westmeyer MD; Rauchfuss TB; Verma AK, Iron Sulfido Derivatives of the Fullerenes C_{60} and C_{70}. Inorg. Chem 1996, 35, 7140–7147. [PubMed: 11666898]
23. Gao W; Yang JYJ, Synthesis and crystal structure of complex (μ-S2)Fe2(CO)4(PPh3)2. Asian J. Chem 2013, 25, 9755–9757.
24. Farrugia LJ; Evans C; Senn HM; Hanninen MM; Sillanpaa R, QTAIM View of Metal-Metal Bonding in Di- and Trinuclear Disulfido Carbonyl Clusters. Organometallics 2012, 31, 2559–2570.
25. Zhuang B; Chen J; He L; Chen J; Zhou Z; Wu K, Synthesis, Structure and Formation Pathways of New Fe–S Complexes Containing [Fe2S2]-Units in Different Valences, $[Fe_2S_2(CO)_4(PPh_3)_2]$, $[Fe_3S_2(CO)_6(PPh_3)_3]$ and $[Fe_4S_2(CO)_{10}]^{2-}$ and the Origin of the $[Fe_2S_2]$-unit in Metal–$[Fe_2S_2(CO)_6]$ Complexes. J. Organomet. Chem 2004, 689, 2674–2683.
26. Liu C; Peck JNT; Wright JA; Pickett CJ; Hall MB, Density Functional Calculations on Protonation of the [FeFe]-Hydrogenase Model Complex $Fe_2(μ\text{-pdt})(CO)_4(PMe_3)_2$ and Subsequent Isomerization Pathways. Eur. J. Inorg. Chem 2011, 1080–1093.
27. Jablonskyte A; Webster LR; Simmons TR; Wright JA; Pickett CJ, Electronic Control of the Protonation Rates of Fe-Fe Bonds. J. Am. Chem. Soc 2014, 136, 13038–13044. [PubMed: 25116589]
28. Zhao X; Georgakaki IP; Miller ML; Mejia-Rodriguez R; Chiang C-Y; Darensbourg MY, Catalysis of H_2/D_2 Scrambling and Other H/D Exchange Processes by [Fe]-Hydrogenase Model Complexes. Inorg. Chem 2002, 41, 3917–3928. [PubMed: 12132916]
29. Savariault J-M; Bonnet J-J; Mathieu R; Galy J, Étude Cristallographique du Composé $\{[(SCH_3)Fe(CO)_2P(CH_3)_2(C_6H_5)]_2H\}^+PF6$-. C. R. Acad. Sci. Paris 1977, 284, 663–667.
30. Barton BE; Zampella G; Justice AK; De Gioia L; Rauchfuss TB; Wilson SR, Isomerization of the Hydride Complexes $[HFe_2(SR)_2(PR_3)_x(CO)_{6-x}]^+$ (x = 2, 3, 4) Relevant to the Active Site Models for the [FeFe]-Hydrogenases. Dalton Trans 2010, 39, 3011–3019. [PubMed: 20221534]
31. Brunner H; Wachter J; Gehart G; Leblanc J-C; Moïse C, Preparation and Reactivity of Peralkylated Tantalocene Sulfur Complexes Having a Fulvenoid Substructure. Organometallics 1996, 15, 1327–1330.
32. Li Q; Lalaoui N; Woods TJ; Rauchfuss TB; Arrigoni F; Zampella G, Electron-Rich, Diiron Bis(monothiolato) Carbonyls: C-S Bond Homolysis in a Mixed Valence Diiron Dithiolate. Inorg. Chem 2018, 57, 4409–4418. [PubMed: 29620876]

33. Song L-C; Zhao P-H; Du Z-Q; Tang M-Y; Hu Q-M, Unexpected Synthesis of Tetrahedral Fe/S Clusters via Highly Reactive Butterfly Intermediates (μ-HS)$_2$Fe$_2$(CO)$_5$[RP(CH$_2$OH)$_2$]. Organometallics 2010, 29, 5751–5753.
34. Keizer PN; Krusic PJ; Morton JR; Preston KF, Thiolato- and Selenato-Bridged Dinuclear Iron Carbonyl Radicals. J. Am. Chem. Soc 1991, 113, 5454–5456.
35. King RB, Organosulfur Derivatives of Metal Carbonyls. I. The Isolation of Two Isomeric Products in the Reaction of Triiron Dodecacarbonyl with Dimethyl Disulfide. J. Am. Chem. Soc 1962, 84, 2460.
36. Mueting A; Mattson BM, Kinetics and Thermodynamics of the Intramolecular Isomerization of [Fe(SCH$_3$)(CO)$_3$]$_2$. J. Inorg. Nucl. Chem 1981, 43, 749–751.
37. Seyferth D; Henderson RS; Song L-C, Chemistry of μ-Dithio-bis(tricarbonyliron), a Mimic of Inorganic Disulfides. 1. Formation of Di-μ-thiolato-bis(tricarbonyliron) Dianion. Organometallics 1982, 1, 125–133.
38. Dahl LF; Wei C-H, Structure and Nature of Bonding of [C$_2$H$_5$SFe(CO)$_3$]$_2$. Inorg. Chem 1963, 2, 328–333.
39. Ortega-Alfaro MC; Hernandez N; Cerna I; Lopez-Cortes JG; Gomez E; Toscano RA; Alvarez-Toledano C, Novel Dinuclear Iron(0) Complexes from a,b-Unsaturated Ketones b-Positioned with Sulfide and Sulfoxide Groups. J. Organomet. Chem 2004, 689, 885–893.
40. Shi Y-C; Wu Z-D; Hou X-L; Li Z-W; Wang Y, Syntheses, Crystal Structures, and Electrochemical Studies of Dinuclear Coordination Compounds with the Fe$_2$(CO)$_6$ Core. J. Coord. Chem 2016, 69, 3603–3618.
41. Song L-C; Zhao Z-Y; Wang J-T, Synthesis and Conformational Analysis of α-Ethoxycarbonylmethyl-Substittuted Sulfur-Bridged Iron Carbonyl Complexes (μ-RS)(μ-EtOC(O)CH$_2$S)Fe$_2$(CO)$_6$. Acta Chim. Sin 1987, 1, 80–84 (Chinese edition **1987**, **19***45*, **1**467—**1**471).
42. Casewit CJ; Coons DE; Wright LL; Miller WK; Rakowski DuBois M, Homogeneous Reductions of Nitrogen-Containing Substrates Catalyzed by Molybdenum(IV) Complexes with μ-Sulfido Ligands. Organometallics 1986, 5, 951–955.
43. Warren JJ; Tronic TA; Mayer JM, Thermochemistry of Proton-Coupled Electron Transfer Reagents and Its Implications. Chem. Rev 2010, 110, 6961–7001. [PubMed: 20925411]
44. Franz JA; Lee S-J; Bowden TA; Alnajjar MS; Appel AM; Birnbaum JC; Bitterwolf TE; Dupuis M, Activation of the S-H Group in Fe(μ$_2$-SH)Fe Clusters: S-H Bond Strengths and Free Radical Reactivity of the Fe(μ$_2$-SH)Fe Cluster. J. Am. Chem. Soc 2009, 131, 15212–15224. [PubMed: 19795866]
45. Gao W; Zhang T-T; Sun Y-J, Synthesis and Structural Characterization of Diiron Ethanedithiolate Complex [(μ-SCH$_2$)$_2$Fe$_2$(CO)$_4$](PPh$_3$)$_2$ Related to the Active Site of [Fe-Fe]-Hydrogenases. Asian J. Chem 2014, 26, 6687–6688.
46. Kramer A; Lingnau R; Lorenz IP; Mayer HA, Komplexchemischer Aufbau cyclischer 1,2-Dithiolato-Liganden mit dem nido Cluster [(CO)$_3$FeS]$_2$. - Molekülstruktur und partielle S-Oxidation von Hexacarbonyl(mu$_2$-cis-1,2-cyclohexandithiolato-S,S}dieisen. Chem. Ber 1990, 123, 1821–1826.
47. Kramer A; Lorenz IP, Photochemisch induzierte [2 + 2]-Cycloadditionen von Alkenen und Dienen mit der S-S-Bindung des *nido*-Clusters [(CO)$_3$FeS]$_2$. J. Organomet. Chem 1990, 388, 187–193.
48. Hieber W; Gruber J, Zur Kenntnis der Eisencarbonylchalkogenide. Z. anorg. allg. Chem 1958, 296, 91–103.
49. Bose KS; Sinn E; Averill BA, Synthesis and X-Ray Structure of the [Fe$_4$S$_4$(CO)$_{12}$]$^{2-}$ Ion: an Example of intermolecular Sisulfide Formation by the (μ-S)$_2$Fe$_2$(CO)$_6$ Unit. Organometallics 1984, 3, 1126–1128.
50. Felton GAN; Mebi CA; Petro BJ; Vannucci AK; Evans DH; Glass RS; Lichtenberger DL, Review of Electrochemical Studies of Complexes Containing the Fe$_2$S$_2$ Core Characteristic of [FeFe]-Hydrogenases Including Catalysis by These Complexes of the Reduction of Acids to Form Dihydrogen. J. Organomet. Chem 2009, 694, 2681–2699.
51. Silaghi-Dumitrescu I; Bitterwolf TE; King RB, Butterfly Diradical Intermediates in Photochemical Reactions of Fe$_2$(CO)$_6$(μ-S$_2$). J. Am. Chem. Soc 2006, 128, 5342–5343. [PubMed: 16620096]

52. Seyferth D; Henderson RS, Photochemically Induced Insertion of Acetylenes into μ-Dithiobis(tricarbonyliron). J. Organomet. Chem 1979, 182, C39–C42.

53. Messelhäuser J; Gutensohn KU; Lorenz IP; Hiller W, Insertionreaktionen von Ethen und Kohlenmonoxid in die S-S Bindung des $[(CO)_3FeS]_2$ *nido*-Clusters und Synthese und Struktur des 1,3-Ethanesulfenatothiolato Complex $[(CO)_3Fe]_2SC_2H_4S(O)$. J. Organomet. Chem 1987, 321, 377–388.

54. Zhao P; Gray DL; Rauchfuss TB, Rational Synthesis of the Carbonyl(perthiolato)diiron $[Fe_2(S_3CPh_2)(CO)_6]$ and Related Complexes. Eur. J. Inorg. Chem 2016, 2016, 2681–2683. [PubMed: 27818613]

55. SAINT SHELXTL, XCIF XPREP, Bruker AXS, Inc, Madison, Wisconsin, 2014.

56. Krause L; Herbst-Irmer R; Sheldrick GM; Stalke D, Comparison of Silver and Molybdenum Microfocus X-Ray Sources for Single-Crystal Structure Determination. J. Appl. Cryst, 2015, 48, 3–10. [PubMed: 26089746]

57. Sheldrick GM, Crystal Structure Refinement with SHELXL. Acta Cryst 2015, C71, 3–8.

58. Sheldrick GM, SHELXT - Integrated Space-Group and Crystal-Structure Determination. Acta Cryst 2015, A71, 3–8.

Synopsis

In contrast with $Fe_2(\mu\text{-}SH)_2(CO)_6$, the complex $Fe_2(\mu\text{-}SH)_2(CO)_4(PPh_3)_2$ exhibits well-behaved anti-oxidant properties resulting from S-centered redox. It reduces TEMPO, O 2, H_2O_2, $(PhCO_2)_2$ and Ph_2N_2 giving $Fe_2(\mu\text{-}S_2)(CO)_4(PPh_3)_2$. Oxidation of $Fe_2(\mu\text{-}SH)_2(CO)_4(PPh_3)_2$ with TEMPO in the presence of C_2H_4 gives the ethanedithiolate $Fe_2(\mu\text{-}S_2C_2H_4)(CO)_4(PPh_3)_2$. Related studies show that the original synthesis of $Fe_2(\mu\text{-}S 2)(CO)_6$ involves protonation of *poly*sulfides $[Fe_2(\mu\text{-}S_n)_2(CO)_6]^{2-}$ ($n > 1$) with elimination of H_2S_x.

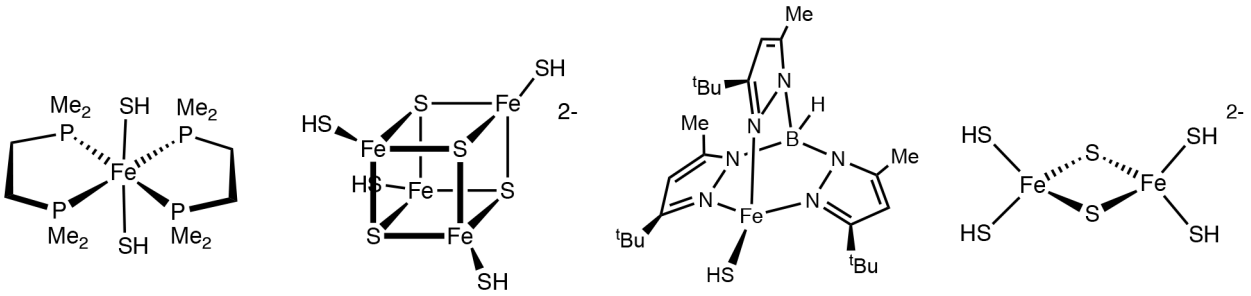

Figure 1.
Structures of selected crystallographically characterized Fe-SH complexes.[16–19]

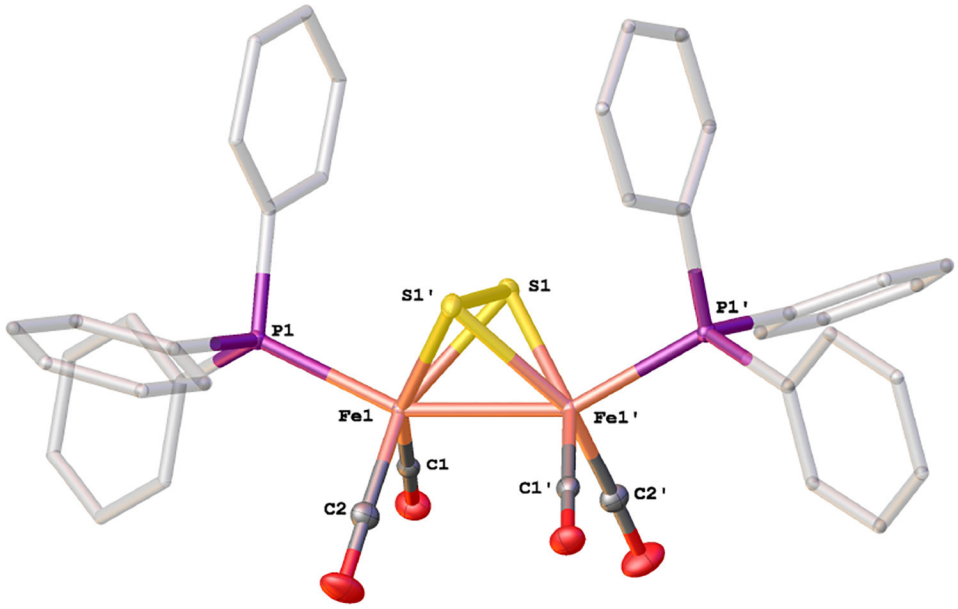

Figure 2.

Structure of $Fe_2(\mu\text{-}S_2)(CO)_4(PPh_3)_2$ (**2**). Selected distances (Å): Fe(1)-Fe(1)', 2.5557(5); Fe(1)-S(1), 2.2391(4); Fe(1)-S(1)', 2.2585(5); Fe(1)'-S(1), 2.2585(5); Fe(1)'-S(1)', 2.2391(4); Fe(1)-P(1), 2.2210(5); Fe(1)'-P(1)', 2.2210(5); S(1)-S(1)', 2.0315(6).

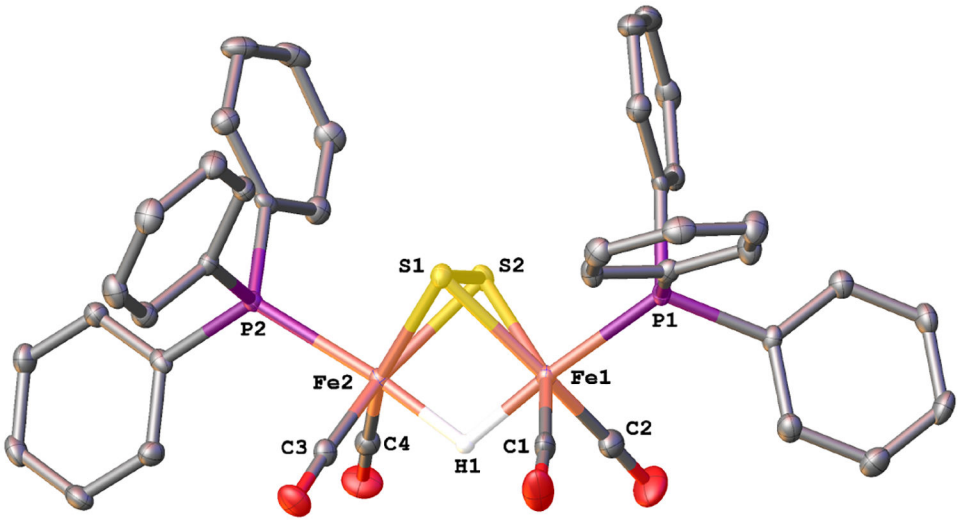

Figure 3.

Structure of the cation in [(μ-H)Fe (μ-S2 2)$(CO)_4(PPh_3)_2$]$BAr^F{}_4$. Selected distances (Å): Fe(1)-Fe(2), 2.6327(6); Fe(1)-S(1), 2.2349(7); Fe(1)-S(2), 2.2565(8); Fe(2)-S(1), 2.2364(7); Fe(2)-S(2), 2.2527(7); Fe(1)-P(1), 2.2570(7); Fe(2)-P(2), 2.2518(8); Fe-CO: 1.788(3)-1.783(3); Fe(1)-H(1): 1.65(4); Fe(2)-H(1): 1.65(3); S(1)-S(2), 2.0201(9).

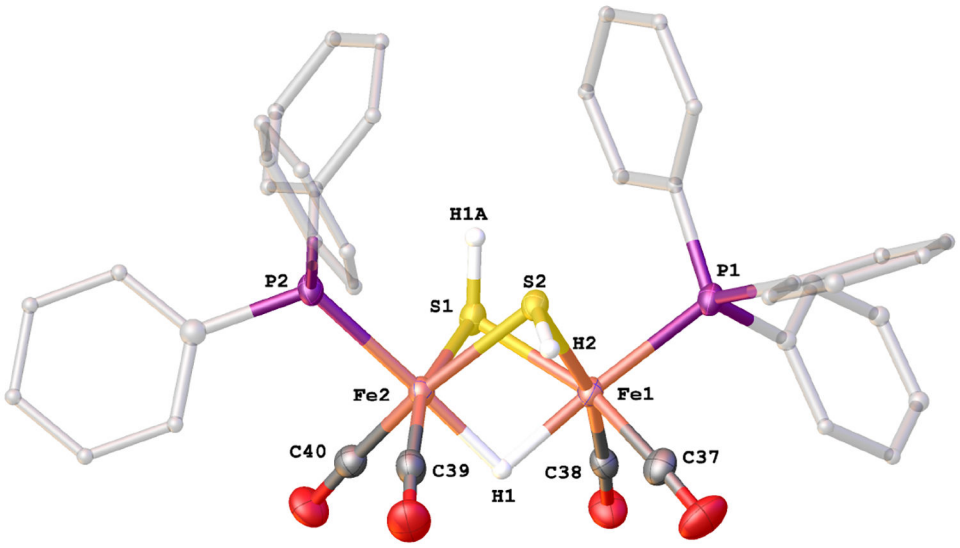

Figure 4.

Structure of the cation in $[(\mu\text{-H})Fe_2(\mu\text{-SH})_2(CO)_4(PPh_3)_2]BAr^F{}_4$. Selected distances (Å): Fe(1)-Fe(2), 2.5893(6); Fe(1)-S(1), 2.2861(9); Fe(1)-S(2), 2.283(1); Fe(2)-S(1), 2.2780(8); Fe(2)-S(2), 2.2679(9); Fe(1)-P(1), 2.2588(9); Fe(2)-P(2), 2.272(1); Fe(1)-H(1): 1.76(4); Fe(2)-H(1), 1.67(4); S(1)-H(1A), 1.21(4); S(2)-H(2), 1.22(3).

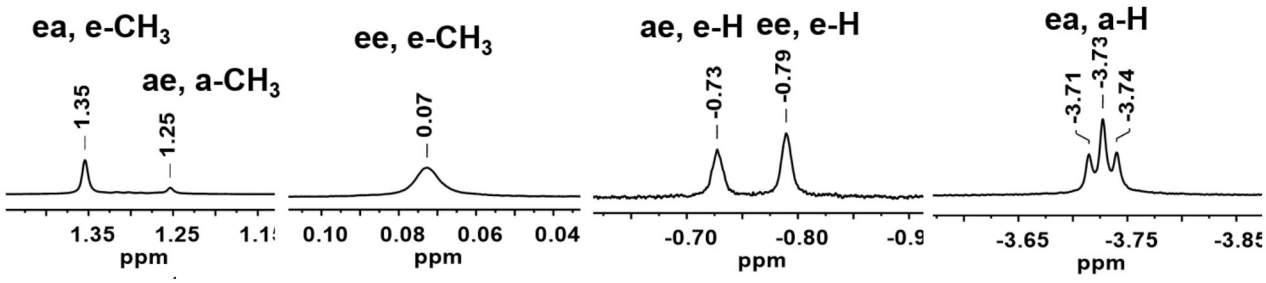

Figure 5.

^{1}H NMR (500 MHz, CD_2Cl_2) spectrum of $Fe_2(\mu\text{-SMe})(\mu\text{-SH})(CO)_4(PPh_3)_2$ at 20°C, depicting expansion of S*Me* and S*H* signals. Three isomers, ae, ee and ea are observed.

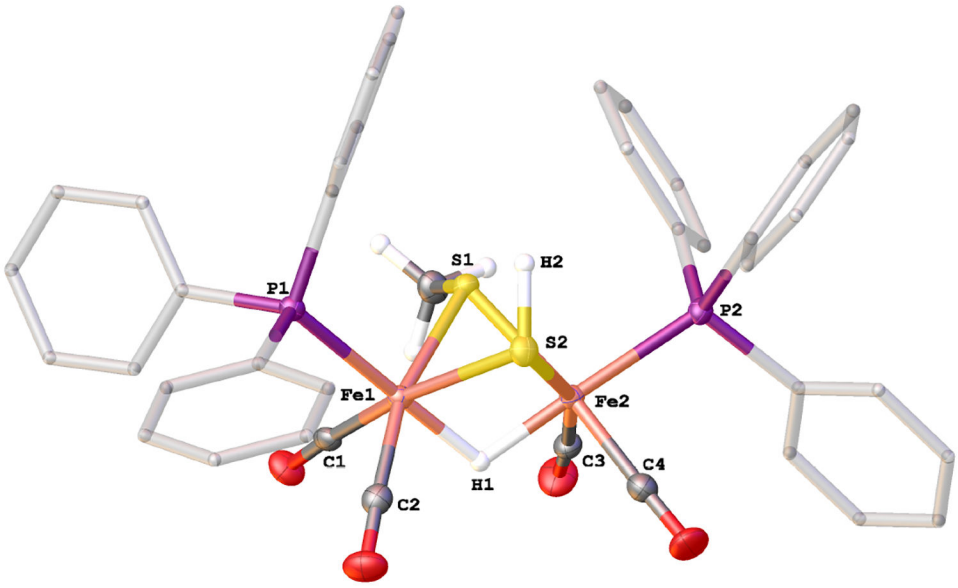

Figure 6.

Structure of the cation in $[(\mu\text{-H})Fe_2(\mu\text{-SH})(\mu\text{-SMe})(CO)_4(PPh_3)_2]BF_4$. Selected distances (Å): Fe(1)-Fe(2), 2.5797(9); Fe(1)-S(1), 2.268(1); Fe(1)-S(2), 2.284(1); Fe(2)-S(1), 2.251(1); Fe(2)-S(2), 2.289(1); Fe(1)-P(1), 2.271(1); Fe(2)-P(2), 2.255(1); Fe(1)-H(1), 1.58(4); Fe(2)-H(1), 1.61(5); S(1)-C(5), 1.818(4); S(2)-H(2), 1.24(4).

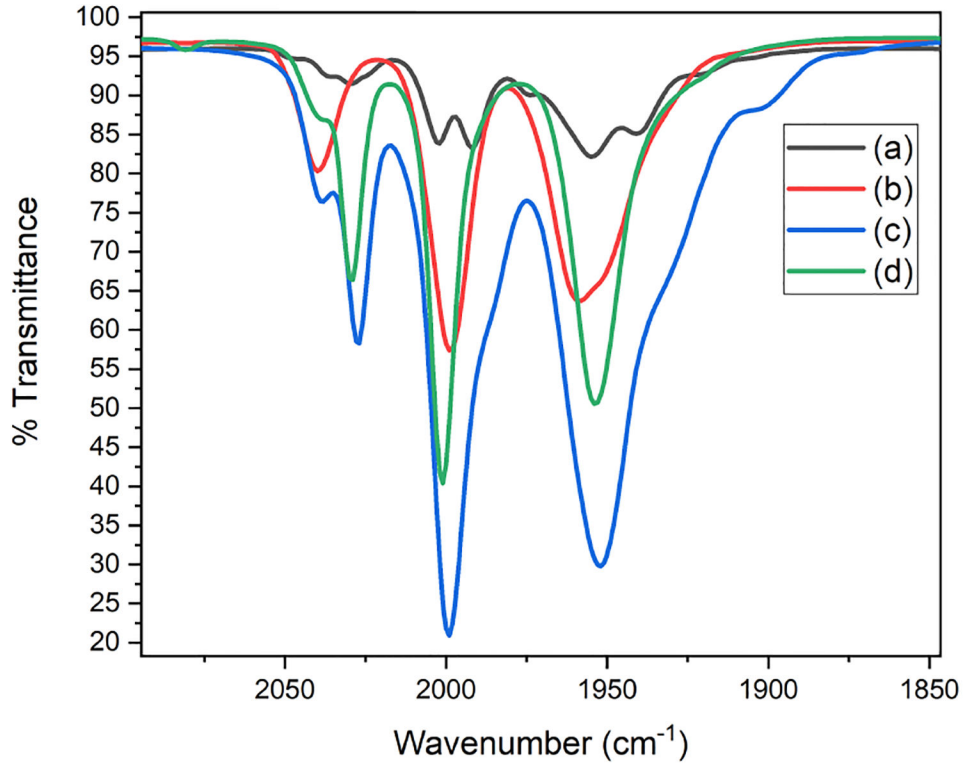

Figure 7.

IR spectra of THF solutions of $Li_2Fe_2S_2(CO)_6$ (a) before and (b) after addition 4 equiv S, (c) the salt precipitated by addition of $BnNMe_3Cl$ to a Hieber-Gruber solution, and (d) $(BnNMe_3)_2[Fe_4S_4(CO)_{12}]$

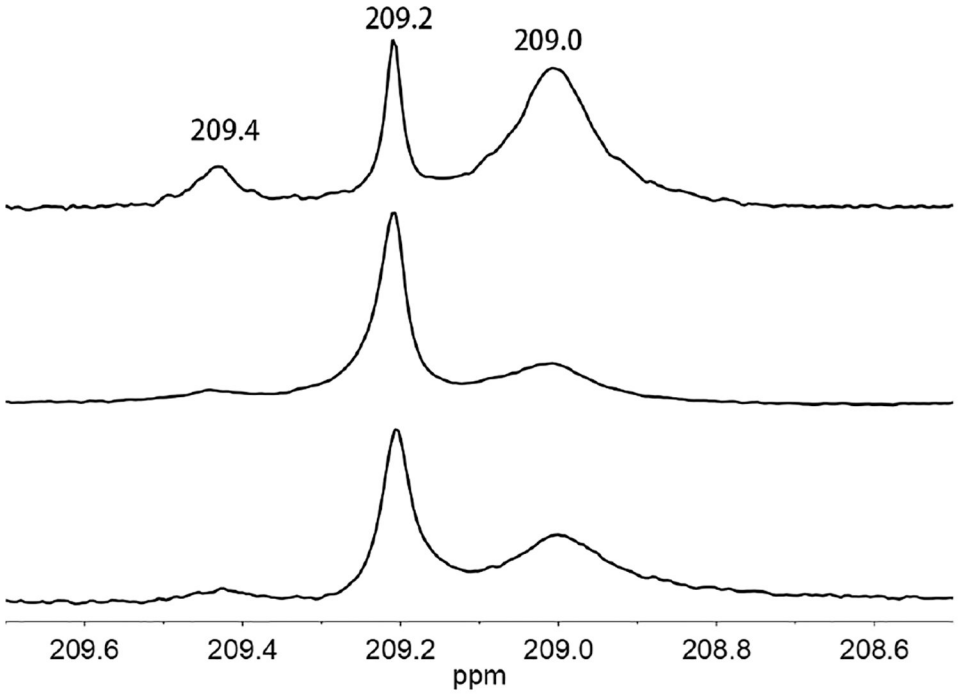

Figure 8.

^{13}C NMR spectra for **1**$^{\mathbf{HH}}$ (top, showing the three isomers), a 1:1 mixture of **1** and **1**$^{\mathbf{HH}}$ (middle), and the pentane-soluble products (bottom) from treatment of acetonitrile solution of $(BnNMe_3)_2[Fe_4S_4(CO)_{12}]$ with 15 equiv of HOTs. All solutions are in CD_2Cl_2 solvent.

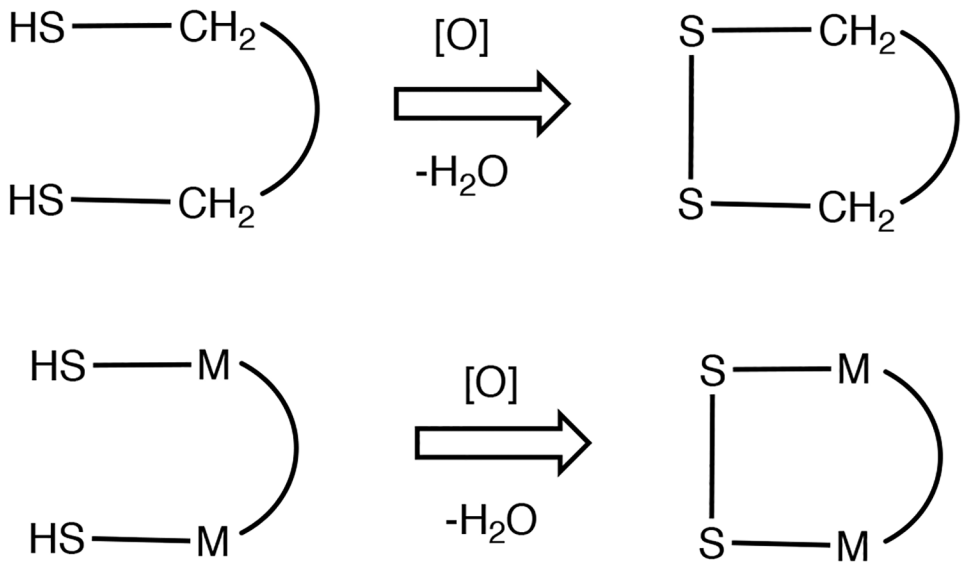

Scheme 1.
Dithiol-Disulfide Antioxidant Reaction.

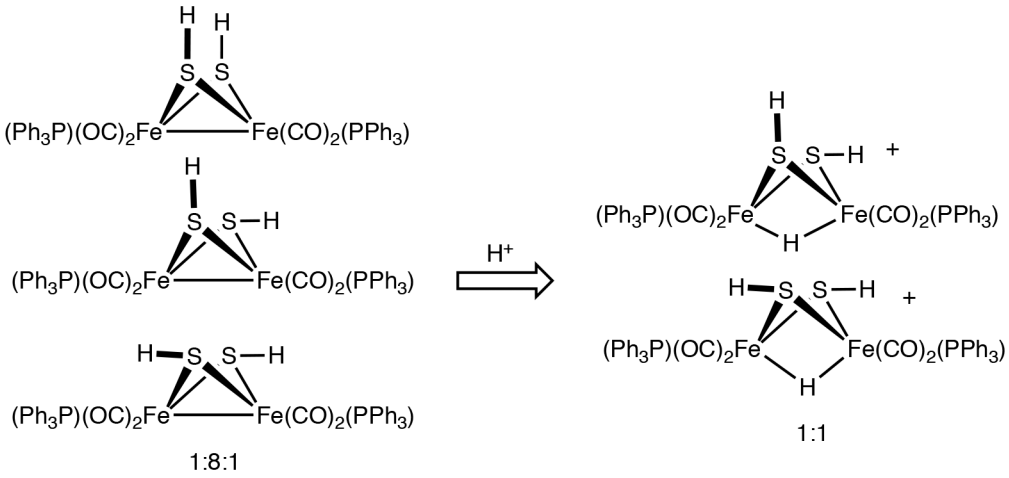

Scheme 2.

Effect of Protonation on Isomerism of the $Fe_2(SH)_2$ Center in **2**$^{\mathbf{HH}}$ and [H**2**$^{\mathbf{HH}}$]$^+$.

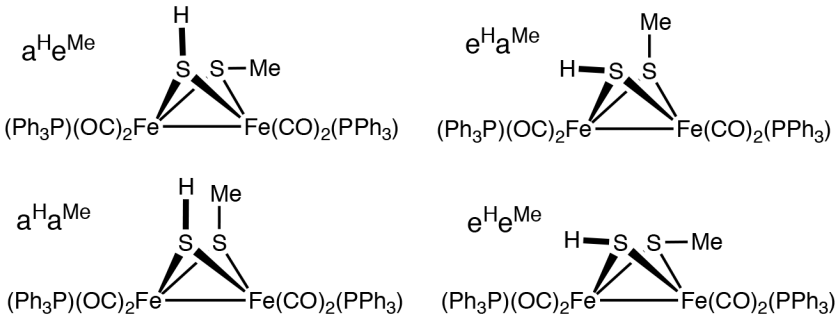

Scheme 3.

Four isomers of **2MeH**. The aHaMe isomer is not observed.

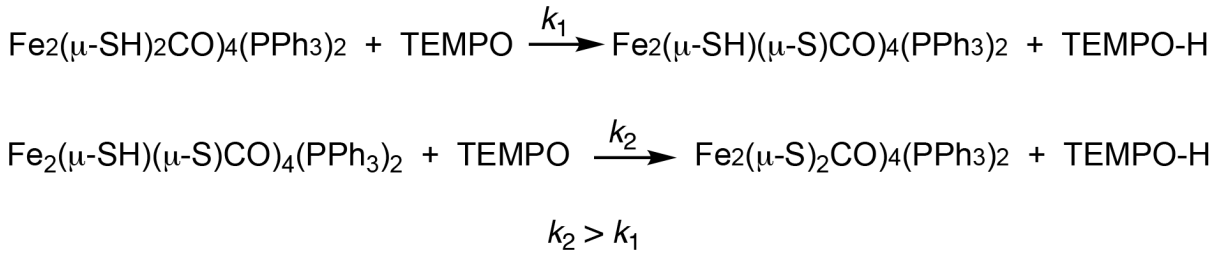

Scheme 4.
Reaction of TEMPO with $\mathbf{2^{HH}}$ and $\mathbf{2^{H}}$.

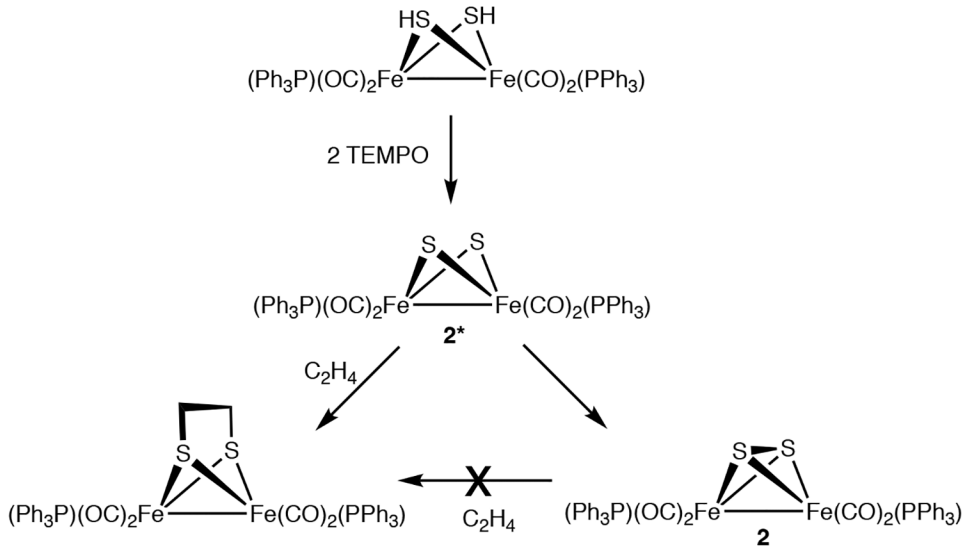

Scheme 5.
Effect of Ethylene on Oxidation of $Fe_2(SH)_2(CO)_4(PPh_3)_2$.

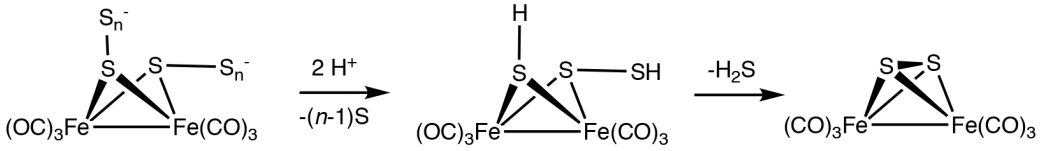

Scheme 6.

Simplified View of the Proposed Final Steps of the Hieber-Gruber Synthesis of **1**.

Table 1.

Selected NMR Data for **1**^{HH}, **3**^{HH}, **2**^{HH}, and **2**^{MeH}.

Complex	NMR Chemical shifts (ppm)		Isomer Ratio (ee:ae:aa)
	^{1}H NMR *SH* Signals (multiplicity, *J* in Hz)	^{31}P NMR	
$Fe_2(\mu\text{-}SH)_2(CO)_6$ (**1**^{HH})	0.3 (s)	-	0.2: 0.7: 0.1
	−0.27 (s), −2.14 (s)		
	−2.25 (s)		
$Fe_2(\mu\text{-}SH)_2(CO)_5(PPh_3)$(**3**^{HH})	0.05 (d, 1.25)	61.2(s)	0.1: 0.8: 0.1
	−0.56 (d, 1.25), −3.01 (d, 5.5)	58.3(s)	
	−3.33 (d, 5.5)	55.8(s)	
$Fe_2(\mu\text{-}SH)_2(CO)_4(PPh_3)_2$(**2**^{HH})	−0.16 (s)	59.2(s)	0.1: 0.8: 0.1
	−0.79 (s), −3.84 (t, 10)	55.2(s)	
	−4.55 (t, 10)	52.2(s)	
$Fe_2(\mu\text{-}SH)(SMe)(CO)_4(PPh_3)_2$(**2**^{MeH})	−0.73 (br s)	57.3 (s)	0.1: 0.8: 0.1
	−0.79 (br s)	55.4 (s)	
	−3.73 (t, 5)	53.1 (s)	

Table 2.

Effect of Fe:*x*S Ratio on the Yields of **1** and $Fe_3S_2(CO)_9$ by the H-G Synthesis Method.

Equiv S	**2.5**	**4.5**	**5.5**	**6.0**	**6.5**	**7.5**	**8.5**	**10**
$Fe_2S_2(CO)_6$	16%	49%	59%	58%	60%	51%	47%	36%
$Fe_3S_2(CO)_9$	37%		0.4%					